NASA TR R-109

N-34

NATIONAL AERONAUTICS AND SPACE ADMINISTRATION

TECHNICAL REPORT

R-109

HYPERSONIC VISCOUS SHOCK LAYER OF NONEQUILIBRIUM DISSOCIATING GAS

By PAUL M. CHUNG

1961

For sale by the Superintendent of Documents, U.S. Government Printing Office, Washington 25, D.C. Yearly subscription, $15: foreign, $19; single copy price varies according to size --------- Price 30 cents

TECHNICAL REPORT R-109

HYPERSONIC VISCOUS SHOCK LAYER OF NONEQUILIBRIUM DISSOCIATING GAS

By PAUL M. CHUNG

Ames Research Center
Moffett Field, Calif.

TECHNICAL REPORT R-109

HYPERSONIC VISCOUS SHOCK LAYER OF NONEQUILIBRIUM DISSOCIATING GAS

By Paul M. Chung

SUMMARY

The nonequilibrium chemical reaction of dissociation and recombination is studied theoretically for air in the viscous shock layer at the stagnation region of axisymmetric bodies. The flight regime considered is for speeds near satellite speed and for altitudes between 200,000 and 300,000 feet.

As altitude is increased from 200,000 to 300,000 feet, the flow in the shock layer varies from one which supports a well-defined boundary layer to one characterized by a thick viscous layer. The chemical reaction rate, at the same time, varies from near equilibrium to completely frozen.

The nonequilibrium chemical reaction is found to produce a significant reduction in the heat transfer to noncatalytic walls at certain altitudes.

It is shown that the controlling chemical reaction for heat transfer at higher altitudes is the dissociative shock-layer reaction, whereas at lower altitudes it is the boundary-layer recombination process.

The effects of nose radius and wall temperature on the heat transfer are studied.

The flight condition at which the air at the boundary-layer edge reaches a state of chemical equilibrium is found.

Also, the simultaneous effect of air rarefaction and nonequilibrium chemical reaction on the shock layer thickness is analyzed.

INTRODUCTION

The flow of chemically reacting gases has been a subject of considerable interest in recent years. The subject became particularly important in external aerodynamics in connection with the calculation of skin friction and heat transfer for hypersonic vehicles. The classical boundary-layer theory usually can be used to analyze skin friction and heat transfer for flights of blunt bodies at altitudes below about 200,000 feet (refs. 1, 2, and 3). For such a flight regime, chemical reaction processes in the inviscid region and in the boundary layer can be studied independently. Studies of the nonequilibrium dissociation and recombination have been carried out by various investigators for the inviscid region (refs. 4 through 6) and for the boundary layer (refs. 7 through 9).

With the current interest in manned space flight and entry into the earth's atmosphere, study of nonequilibrium aerodynamics must be extended beyond 200,000 feet altitude. This is true because the maximum convective heating for many blunt-nosed vehicles returning to the earth from parabolic orbits may occur at altitudes above 200,000 feet (ref. 10). In addition to the problem of convective heat transfer, an understanding of the chemical reaction in the entire shock layer near the stagnation region is very important in the analysis of radiative heat transfer, communication, and re-entry trails (refs. 11 and 12). The study of the nonequilibrium viscous shock layer becomes increasingly complicated as altitudes are increased above about 200,000 feet because the inviscid and the viscous flow regimes can no longer be analyzed separately. The complication is due to the interaction of vorticity and chemical reaction in the zone between the shock layer and the boundary layer.

The viscous shock layer in the rarefied atmosphere between the altitudes of 200,000 feet and 300,000 feet was studied in references 1, 2, and 3 with the air assumed to be chemically inert. The analysis showed that, at the stagnation region of spheres, the skin friction and heat transfer are much higher than those calculated by classical boundary-layer theory in the range of $10^3 \leqq Re \leqq 10^5$. These Reynolds numbers roughly correspond to

the flight regime of present interest for blunt bodies with nose radii between 1 and 5 feet.

In the present paper, the chemical reaction of nonequilibrium dissociation and recombination in the viscous shock layer will be studied, and the effect of the chemical reaction on stagnation point heat transfer will be investigated for noncatalytic walls. The flight regime of the blunt bodies considered in the present study is for altitudes between 200,000 feet and 300,000 feet and for flight speeds near satellite speed.

As will be seen in the text, the actual numerical solutions of the governing equations require considerable care because of the complications imposed by the nonequilibrium effect. In order not to further complicate the numerical phase of the analysis, certain simplifying assumptions will be made on the fluid properties.

SYMBOLS

a speed of sound
B constant defined by equation (A8)
c atom mass fraction
c_i mass fraction of ith species
c_c complementary solution of equation (A1) and solution of equation (A4)
c_p particular solution of equation (A1) and solution of equation (A5)
E_n energy of the nth electronic state
f dimensionless stream function defined by equations (41) and (42)
g_n degeneracy of the nth electronic state
H $\dfrac{h}{u_\infty^2/2}$
h static enthalpy of air including chemical energy ($\approx h_t$ in the shock layer)
h_i static enthalpy of ith species
h_i° heat of formation of ith species
Δh° heat of dissociation
h_t total enthalpy defined by equation (15)
$\hat{h}$ Plank constant
I molecular moment of inertia
j 0 for two-dimensional bodies; 1 for axisymmetric bodies
K curvature of the body surface
K_p equilibrium constant based on partial pressures
k Boltzmann constant
k_r specific recombination coefficient
L nose radius
l characteristic length
M Mach number
M_i molecular weight of ith species
m_i mass of ith particle
N total number of particles
n 1, 2, 3, . . .
p pressure
Pr Prandtl number
Q_i total partition function of ith species
$Q_{i,e}$ electronic partition function of ith species
$Q_{i,r}$ rotational partition function of ith species
$Q_{i,t}$ translational partition function of ith species
$Q_{i,v}$ vibrational partition function of ith species
q heat-transfer rate to wall per unit area
R universal gas constant
Re free-stream Reynolds number, $\dfrac{\rho_\infty u_\infty L}{\mu_\infty}$
T absolute temperature
u x component of velocity
u_1 x component of velocity gradient
u_∞ free-stream velocity
v y component of velocity
W production rate of atoms by chemical reaction per unit volume
X_i mole concentration of ith species
x direction parallel to wall (see fig. 1)
y direction normal to wall (see fig. 1)
β_0 streamwise velocity gradient at the boundary-layer edge
Γ constant used in the appendix
Δ shock-layer thickness
ϵ density ratio across shock, $\dfrac{\rho_\infty}{\rho_s}$
η similarity variable defined by equation (40)
θ_D characteristic temperature of dissociation
θ_v characteristic vibrational temperature
λ mean free path
μ dynamic coefficient of viscosity
μ' dilatational coefficient of viscosity
μ'' longitudinal coefficient of viscosity
ρ density

SUBSCRIPTS

AE adiabatic equilibrium, the value which would be obtained if the air were allowed to reach equilibrium adiabatically with h_s
BL boundary layer
E local equilibrium
i ith species
n nth state or nth iteration
s immediately behind shock

SL shock layer
w wall
1 atoms
2 molecules
3 third body which is either atom or molecule
∞ free stream

SUPERSCRIPT

$'$ total differentiation with respect to η

SHOCK-LAYER CONSERVATION EQUATIONS

In the present analysis, the simplified forms of the Navier-Stokes equation and the corresponding energy and diffusion equations will be used in conjunction with the no-slip wall conditions and the conventional shock relations. We shall first try to justify the use of the equations and the wall and shock conditions for the flight regime of altitudes between 200,000 feet and 300,000 feet and for Mach numbers of near 30. We shall then develop the appropriate conservation equations and boundary conditions.

In 1946, Tsien (ref. 13) first proposed a classification of fluid mechanics based on the Knudsen number. Knudsen number expresses the degree of rarefaction of the fluid and is defined as the ratio of the mean free path to a characteristic length, λ/l. Of the various regimes into which Tsien and others catagorized gasdynamics, in general, only two are reasonably well defined. They are the regime of ordinary continuum gasdynamics wherein the density is sufficiently high that intermolecular collisions dominate over collisions with the boundaries, and the regime of free molecule flow where the gas is sufficiently rarefied that collisions with the boundaries dominate over colisions between the molecules. In terms of the Knudsen number, the two regions are characterized by the inequalities $\lambda/l<<1$ and $\lambda/l>>1$, respectively.

Since 1946, considerable theoretical work has been done on the subject of free molecule flow (see, e.g., ref. 14). The problem of free molecule flow was first attacked because the classical kinetic theory could be applied to this limiting case more readily than to the intermediate regimes.

In recent years, the intermediate regime has been studied with new interest and, as a consequence, some promising theories have been formulated and a few interesting solutions have been obtained. Some of this work appears in references 1, 2, 3, and 15. The recent success in studying the intermediate range of rarefied gasdynamics was made possible by the continuum approach which utilizes the Navier-Stokes equation. Probstein and Kemp in reference 1 subdivided the entire flow regime, between the boundary-layer regime and the free molecule regime, into seven subregimes: boundary-layer regime, vorticity interaction regime, viscous-layer regime, incipient merged layer regime, fully merged layer regime, first-order collision theory regime, and free molecule flow regime. Probstein and Kemp suggested that the Navier-Stokes equation be used through the fully merged layer regime for engineering purposes. Moreover, through the viscous-layer regime, the shock wave near the stagnation region may be considered as a finite discontinuity and the conventional shock relationships may be used to predict the flow conditions immediately behind the shock wave. The justifications for these suggestions are found in references 1 and 15. We shall here briefly recapitulate the portions of the arguments which are directly pertinent to the present work.

We shall first show that the flight regime of present interest lies in the continuum and the viscous-layer regimes. In the present paper, we are interested in the shock layer at the stagnation region of axisymmetric bodies only. The mean free path and the characteristic length of concern are, then, those in the shock layer itself. In order that the continuum theory be valid in the present study, we must have $(\lambda_{SL}/\Delta)<<1$. The mean free path λ_{SL} is longest immediately behind the shock wave where the effect of the cooled wall is not felt. We shall, therefore, justify the continuum theory on the basis of the mean free path immediately behind the shock to be on the safe side. The continuum theory is then valid when

$$\frac{\lambda_s}{\Delta}<<1 \tag{1}$$

With the aid of kinetic theory, we have

$$\lambda_s \sim \frac{\mu_s}{\rho_s a_s} \tag{2}$$

$$\frac{\mu_s}{\mu_\infty} \sim \frac{a_s}{a_\infty} \sim \sqrt{\frac{T_s}{T_\infty}} \tag{3}$$

With the aid of equations (2) and (3), the continuum criterion (1) becomes

$$\frac{M_\infty}{Re}<<1 \tag{4}$$

The conventional shock relations can be used, in general, if the conductive process expressed by $\mu_s(\partial u/\partial y)_s$ is much smaller than the convective process given by $\rho_s u_s v_s$ at the shock wave. With the aid of the assumptions $(\partial u/\partial y)_s \sim u_s/\Delta$ and $a_s \sim \sqrt{\epsilon}\, u_\infty$, it can be shown that the magnitude of the conductive process becomes much smaller than that of the convective process when

$$\frac{M_\infty}{Re}<<\sqrt{\epsilon} \tag{5}$$

Now consider a body with a nose radius of 1 foot traveling at the speed of $M_\infty=30$. At the altitudes of 250,000 and 300,000 feet, the free-stream Reynolds numbers are in the order of 10^4 and 10^3, respectively. The ratio M_∞/Re is, therefore, of the orders of 0.003 and 0.03, respectively. The density ratio ϵ is the order of 0.1 at these flight conditions. It is seen, therefore, that the continuum condition (4) and the viscous layer condition (5) are satisfied at the stagnation point of axisymmetric bodies for flight altitudes below about 300,000 feet.

Next we shall show that the satisfaction of the continuum criterion (4) automatically validates the no-slip wall conditions for a cooled wall. The velocity jump at the wall can be expressed as:

$$u(o)=\lambda_w\left(\frac{\partial u}{\partial y}\right)_w \tag{6}$$

The effect of slip will be negligible in the solutions of the present problem if

$$u(o)<<u_s \tag{7}$$

At the rarefied condition where slip may begin to occur, the shear stress $\mu(\partial u/\partial y)$ will be of the same order of magnitude all along the stagnation stream line from the body to the shock. Inequality (7) becomes, with the aid of the relationships (2), (3), and (6)

$$\frac{M_\infty}{Re}<<\sqrt{\frac{T_s}{T_w}} \tag{8}$$

For the present case of $T_w<<T_s$, $\sqrt{T_s/T_w}>1$ and, therefore, condition (8) is automatically met when the continuum criterion (4) is satisfied. It is seen, therefore, that slip is not an important phenomenon in the stagnation region in affecting skin friction and heat transfer.

Now it is seen that, for the flight regime of present interest, we may use the Navier-Stokes equation and the corresponding forms of the energy and diffusion equations to study the viscous shock layer at the stagnation region of axisymmetric bodies. It is also seen that the no-slip wall conditions and the conventional shock relationships may be applied to the present case.

In the remainder of this section we shall develop a set of shock-layer conservation equations. Though the development given is brief, the casual reader may skip over to the final form of the conservation equations, (18) through (28). Aside from the nonequilibrium chemical effect, the equations used in the subsequent portion are similar to those developed in reference 15.

For a reasonably thin shock layer over two-dimensional and axisymmetric bodies, the Navier-Stokes, the energy, and the diffusion equations can be written in the following simplified form for a boundary-layer-type coordinate system. (See fig. 1 for the coordinate system.)

Continuity:

$$\frac{\partial \rho u}{\partial x}+\frac{j\rho u}{x}+\frac{\partial \rho v}{\partial y}+(1+j)K\rho v=0 \tag{9}$$

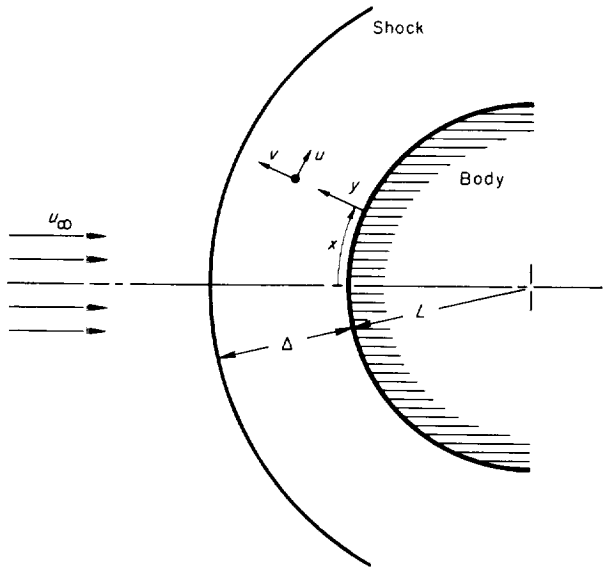

FIGURE 1.—Physical model considered.

x component of momentum

$$u\frac{\partial u}{\partial x}+v\frac{\partial u}{\partial y}+Kuv+\frac{1}{\rho}\frac{\partial p}{\partial x}=\frac{1}{\rho}\frac{\partial}{\partial y}\left(\mu\frac{\partial u}{\partial y}\right) \quad (10)$$

y component of momentum

$$u\frac{\partial v}{\partial x}+v\frac{\partial v}{\partial y}-Ku^2+\frac{1}{\rho}\frac{\partial p}{\partial y}=\frac{1}{\rho}\frac{\partial}{\partial y}\left(\mu''\frac{\partial v}{\partial y}\right)$$
$$+\frac{1}{\rho}\frac{\partial}{\partial y}\left[\left(\mu'-\frac{2}{3}\mu\right)\frac{\partial u}{\partial x}\right]+\frac{\mu}{\rho}\frac{\partial^2 u}{\partial x\partial y} \quad (11)$$

Energy

$$u\frac{\partial h_t}{\partial x}+v\frac{\partial h_t}{\partial y}=\frac{1}{\rho}\frac{\partial}{\partial y}\left(\frac{\mu}{Pr}\frac{\partial h}{\partial y}+\mu''v\frac{\partial v}{\partial y}\right) \quad (12)$$

Diffusion

$$u\frac{\partial C}{\partial x}+v\frac{\partial C}{\partial y}=\frac{1}{\rho}\frac{\partial}{\partial y}\left(\frac{\mu}{Pr}\frac{\partial C}{\partial y}\right)+\frac{W}{\rho} \quad (13)$$

where

$$h_t=h+\frac{u^2+v^2}{2} \quad (14)$$

$$=\Sigma C_i h_i+\frac{u^2+v^2}{2} \quad (15)$$

Lewis number is assumed to be unity in the energy and diffusion equations. In the derivation of the diffusion equation (13), the air is assumed to be a molecule-atom binary mixture and the effect of thermal diffusion is neglected. The justification for neglecting the thermal diffusion effect is as follows. First of all, the effect of thermal diffusion is negligible compared to that of concentration diffusion at temperatures below about 10,000° K (refs. 7 and 15). The effect of thermal diffusion is, therefore, not important near the cooled wall. Near the shock wave, on the other hand, the temperature may be considerably higher than 10,000° K. The convective process, however, predominates over the conductive process near the shock wave since condition (5) is met in the present flight regime. Thermal diffusion is, therefore, neglected in the present study.

Now, for the purpose of simplicity, we shall make the assumption that the shock layer is very thin, so that

$$\frac{\partial p}{\partial y}=0 \quad (16)$$

The above assumption makes the results of the subsequent analysis quite restrictive. The assumption, however, should not cause any undue errors in the present analysis which is concerned with extremely large Mach numbers only. The following order-of-magnitude arguments are now used to simplify the equations further.

$$\left.\begin{aligned}\frac{\Delta}{L}\sim\frac{\rho_\infty}{\rho}\sim\frac{v}{u_\infty}\sim\frac{\mu}{\rho_\infty u_\infty L}\sim\epsilon\\ \frac{p}{\rho_\infty u_\infty^2}\sim\frac{h_t}{u_\infty^2}\sim 1\end{aligned}\right\} \quad (17)$$

Guided by experience with stagnation-point boundary layer work, it is assumed that all the fluid properties and the dependent variables, except the x component of the velocity and pressure, are functions of y only. The velocity component u is expressed as $u=u_1(y)x$, and also, the variation of pressure in the x direction is expressed by Newtonian theory. The conservation equations (9) through (13) are now simplified for a sphere as:

Continuity

$$2\rho u_1+\frac{d\rho v}{dy}=0 \quad (18)$$

Momentum

$$u_1^2+v\frac{du_1}{dy}-\frac{2p}{\rho L^2}=\frac{1}{\rho}\frac{d}{dy}\left(\mu\frac{du_1}{dy}\right) \quad (19)$$

Energy

$$v\frac{dh}{dy}=\frac{1}{\rho}\frac{d}{dy}\left(\frac{\mu}{Pr}\frac{dh}{dy}\right) \quad (20)^1$$

Diffusion

$$v\frac{dC}{dy}=\frac{1}{\rho}\frac{d}{dy}\left(\frac{\mu}{Pr}\frac{dC}{dy}\right)+\frac{W}{\rho} \quad (21)$$

The equation of state is

$$p=\rho(1+C)\frac{R}{M_2}T \quad (22)$$

The boundary conditions are as follows: At the wall ($y=0$),

$$u_1=v=0 \quad (23)$$

$$h=h_w \quad (24)$$

$$\frac{dC}{dy}=0 \text{ (noncatalytic wall)} \quad (25)$$

[1] In the shock layer, $(u^2+v^2)/2<<h$; therefore we let $h_t=h$.

at the shock wave ($y=y_s$),

$$u_1=\frac{u_\infty}{L},\ v=-\frac{\rho_\infty u_\infty}{\rho_s} \tag{26}$$

$$h=\frac{u_\infty^2}{2} \tag{27}$$

$$C=0 \tag{28}$$

As shown by the boundary condition (25), the wall is considered to be noncatalytic. Also, the chemical reaction is considered to be frozen through the shock wave and, therefore, the boundary condition (28) is valid.

The conservation equations and the boundary conditions, equations (18) through (28), will become complete and ready for solution as soon as the expression for the chemical reaction rate term W/ρ becomes known. In the next section, the gas model and the chemical reaction kinetics will be discussed. A simplified expression for the enthalpy, h, and the expression for the chemical reaction rate W/ρ will be derived.

GAS MODEL AND CHEMICAL REACTION

In the present section, the gas model and the chemical reaction will be discussed for the air in the shock layer. As a consequence, the simplified expression for the enthalpy and an expression for the chemical reaction rate will be derived.

For simplicity, we shall consider that the air in the shock layer is a binary mixture of air atoms and air molecules. We shall assume that the rotational and the vibrational degrees of freedom are in equilibrium with the translational degree of freedom at all times. All the electronic degrees of freedom, on the other hand, are assumed to be unexcited, and it is also assumed that ionization is negligible. The nonequilibrium phenomena considered are, therefore, those of dissociation and recombination only.

The rotational degree of freedom probably is in equilibrium with the translational degree of freedom. The vibrational temperature, on the other hand, may lag behind the translational temperature because of the rather long vibrational relaxation time near the shock wave. The vibrational relaxation, under such circumstances, may be coupled with the dissociative relaxation, and the two relaxation phenomena may occur simultaneously near the shock wave. The addition of the simultaneous relaxation phenomenon increases the complexity of the solution considerably; therefore, we shall leave this phenomenon to a later study. The effect of finite vibrational relaxation, however, should not alter the present results greatly since the thermal effect associated with the vibrational mode of freedom is much less than that associated with dissociation and recombination. The electronic states probably will be excited to some degree at the elevated temperature near the shock wave. The excitation of the electronic states affects the present problem basically through its effect on the partition functions. A study of the partition functions of oxygen and nitrogen atoms and molecules showed that the contribution of the fully excited electronic states to the partition functions is very small compared to that of the other degrees of freedom (see ref. 16). The assumption of unexcited electronic states may be justified here for engineering purposes. Finally, there could be some ionization of the hot air molecules near the shock wave. Most of the ionization, however, will probably take place following the dissociation. The temperature will decrease rapidly with dissociation and this will tend to decrease the ionization. At present, nothing can be said with any certainty on the amount of ionization which may be present at the high temperatures mainly because of the lack of information on high temperature ionization reaction kinetics. Moreover, the presence of a large amount of ionization will invalidate the present conservation equations. In the present study we shall neglect ionization completely and, at the same time, limit the analysis to the flight speeds up to about 30,000 ft/sec.

Now with the use of the above mentioned simplifications, we shall develop the expressions for the enthalpy and the chemical reaction rate.

In order to obtain the properties of the air, we must first obtain the total partition functions for the atoms and the molecules. Making the usual assumption that no coupling exists between the different modes of energy, we have,

$$Q_i=Q_{t,t}Q_{t,r}Q_{t,v}Q_{t,e} \tag{29}$$

The general expressions of the partial partition functions can be obtained from the standard literature on statistical mechanics (e.g., refs. 16 and 17). They are:

$$\left.\begin{aligned} Q_{i,t}&=\left(\frac{2\pi m_i kT}{\hat{h}^2}\right)^{3/2}\frac{RT}{p}\\ Q_{1,r}&=0\\ Q_{2,r}&=\frac{4\pi^2 IkT}{\hat{h}^2}\\ Q_{1,v}&=0\\ Q_{2,v}&=\frac{1}{1-e^{-\theta_v/T}}\\ Q_{i,e}&=\Sigma g_n e^{-E_n/kT}\end{aligned}\right\} \tag{30}$$

The enthalpy of the fluid is obtained by the equation

$$h=\Sigma C_i h_i=\Sigma C_i\left[\frac{R}{M_i}T^2\left(\frac{\partial \ln Q_i}{\partial T}\right)_p+h_i^\circ\right] \tag{31}$$

For the present atom-molecule binary mixture with unexcited electronic states, equation (31) becomes with the aid of equations (30):

$$h=\left[\frac{7}{2}+\frac{3}{2}C+(1-C)\left(\frac{\theta_v/T}{e^{\theta_v/T}-1}\right)\right]\frac{R}{M_2}T+C\Delta h^\circ \tag{32}$$

The term $(1-C)[(\theta_v/T)/(e^{\theta_v/T}-1)]$ in equation (32) represents the contribution of the vibrational degree of freedom of the molecules to the enthalpy. The value of the term varies from 0 to $(1-C)$ as the temperature is varied from absolute zero to infinity. The contribution of the vibrational degree of freedom to enthalpy is maximum when $C=0$. The maximum contribution, according to equation (32), is about 20 percent of the total enthalpy, provided no abnormal vibrational excitations exist. The value of the term, $(\theta_v/T)/(e^{\theta_v/T}-1)$, becomes practically unity at a temperature of about 4000° K. Lighthill, in reference 18, set $(\theta_v/T)/(e^{\theta_v/T}-1)=1/2$ because the maximum temperature considered was not much above 4000° K. In the flight regime of present interest, however, the maximum temperature is much higher than 4000° K, and most of the chemical reactions take place at temperatures above 4000° K. We shall, therefore, set $(\theta_v/T)/(e^{\theta_v/T}-1)=1$ in the present analysis. Equation (32) now becomes

$$h=\left(\frac{9}{2}+\frac{1}{2}C\right)\frac{R}{M_2}T+C\Delta h^\circ \tag{33}$$

600421—61——2

The molecular weight and the heat of dissociation of air used in the subsequent numerical work are the weighed average values of O_2 and N_2.

The type of chemical reaction considered in the present paper is:

$$X_1+X_1+X_3\rightleftarrows X_2+X_3 \tag{34}$$

For the chemical reaction expressed by equation (34), the applications of the law of mass action and the equation of state yield the following equation for the reaction rate:

$$\frac{W}{\rho}=-2(2k_r)\left(\frac{p}{RT}\right)^2\left[\frac{C^2}{1-C}-\frac{1}{4_p}K_p(1-C)\right] \tag{35}$$

In order for equation (35) to be quantitatively useful, the equilibrium constant K_p and the specific recombination coefficient k_r must be known.

The equilibrium constant can be quite accurately calculated by the use of the partition functions. At chemical equilibrium, the concentrations of the species are given by the following equation (see refs. 16 and 17):

$$\frac{(\text{number of atoms})^2}{\text{number of molecules}}=\frac{Q_1^2}{Q_2}e^{-\theta_D/T} \tag{36}$$

The equilibrium constant for the reaction shown by equation (34) is then derived from equation (36) as

$$K_p=\frac{p}{N}\frac{Q_1^2}{Q_2}e^{-\theta_D/T} \tag{37}$$

The specific expanded expressions for the partial partition functions, equations (30), are given for the atoms and molecules of oxygen and nitrogen in reference 16. The expressions given in reference 16 are for temperatures up to only 15,000° K. With the present assumption of unexcited electronic states, however, these expressions can be used in the present study even for temperatures much above 15,000° K. The specific properties, such as θ_v, θ_D, etc., used in the subsequent numerical work are the weighed average values of oxygen and nitrogen.

The exact values of the specific recombination coefficient k_r are not so readily obtainable by a theoretical treatment alone. All the reliable experimental data available so far are limited to temperatures up to about 7000° K. Experimental results of specific recombination coefficients are reported in references 19 and 20 for oxygen and

nitrogen for temperatures up to about 7000° K. The results showed that the recombination coefficients varied with the third body which acts as a catalyst in the chemical reaction. A study of the experimental results of the references and those obtained by other investigators showed that the specific recombination coefficient for the air in the shock layer, a mixture of atoms and molecules of oxygen and nitrogen, could be represented reasonably well by the equation

$$2k_r=1.56\times10^{20}\left(\frac{1}{T}\right)^{1.5}\frac{\text{cm}^6}{\text{mole}^2\text{sec}} \tag{38}$$

The same recombination coefficient given by the above equation was also used in the boundary-layer work of reference 9.

The reaction rate, W/ρ, given by equation (35) now becomes, with the aid of equations (37) and (38),

$$\frac{W}{\rho}=-2(1.56\times10^{20})\left(\frac{1}{T}\right)^{1.5}\left(\frac{p}{RT}\right)^2\left[\frac{C^2}{1+C}-\frac{1}{4p}\left(\frac{p}{N}\frac{Q_1^2}{Q_2}e^{-\theta_D/T}\right)(1-C)\right] \tag{39}$$

where T and p are in degrees Kelvin and atmospheres, respectively.

SOLUTION OF CONSERVATION EQUATIONS AND HEAT TRANSFER

We shall, in the present section, solve the governing equations, (18) through (21), with their boundary conditions for the velocity, enthalpy, temperature, atom concentration distributions, and shock-layer thickness. As a consequence of the solution, we shall then obtain the heat transfer to the stagnation point of spheres.

The principles involved in solving the equations are rather straightforward. A boundary-layer-type affine transformation will be performed on the governing equations (18) through (21) and on their boundary conditions. The simultaneous ordinary differential equations thus obtained will then be solved numerically by the use of a digital computer. Though the principles involved are rather simple, the actual solution of the equations is quite complicated. The equations are strongly nonlinear and coupled. Moreover, the shock-wave detachment distance at which one set of the boundary conditions must be applied is not known a priori. In order to make the equations converge satisfactorily, a rather compounded iteration procedure is used. The transformed conservation equations and the expression for the heat transfer will be developed in the present section. The method of iteration and the numerical solution will be discussed in the appendix.

We first define a similarity variable for the case of a sphere as

$$\eta=\sqrt{\frac{2^{1/2}(u_\infty/L)}{\rho_s\mu_s}}\int_0^y\rho\,dy \tag{40}$$

We then express the streamwise velocity gradient u_1 and the normal velocity component v as follows:

$$u_1=\sqrt{2}\left(\frac{u_\infty}{L}\right)f'(\eta) \tag{41}$$

$$v=-2^{3/2}\left(\frac{u_\infty}{L}\right)f(\eta)\left(\frac{dy}{d\eta}\right) \tag{42}$$

At the stagnation point of the axisymmetric body, the continuity equation (18) is automatically satisfied by the particular definition of $f(\eta)$. The momentum, energy, and diffusion equations, equations (19), (20), and (21), are transformed as follows with the assumption of a constant Prandtl number:

Momentum

$$\left[\left(\frac{\rho\mu}{\rho_s\mu_s}\right)f''\right]'+2ff''+\left(\frac{\rho_\infty}{\rho}-f'^2\right)=0 \tag{43}$$

Energy

$$\frac{1}{Pr}\left[\left(\frac{\rho\mu}{\rho_s\mu_s}\right)H'\right]'+2fH'=0 \tag{44}$$

Diffusion

$$\frac{1}{Pr}\left[\left(\frac{\rho\mu}{\rho_s\mu_s}\right)C'\right]'+2fC'=-\frac{1}{\sqrt{2}}\left(\frac{L}{u_\infty}\right)\left(\frac{W}{\rho}\right) \tag{45}$$

The reaction rate W/ρ is given by equation (39). The equation of state (22) and the expression of enthalpy given by equation (33) constitute two additional equations. The boundary conditions (23) through (28) become: at $\eta=0$

$$f=f'=0 \tag{46}$$

$$H=H_w=\frac{\left(\frac{9}{2}+\frac{1}{2}C_w\right)\frac{R}{M_2}T_w+C_w\Delta h^\circ}{\frac{u_\infty^2}{2}} \tag{47}$$

$$C'=0 \tag{48}$$

at $\eta=\eta_s$

$$f=2^{-5/4}\sqrt{\frac{u_\infty L}{\rho_s\mu_s}}\rho_\infty \tag{49}$$

$$f'=\frac{1}{\sqrt{2}} \tag{50}$$

$$H=1 \tag{51}$$

$$C=0 \tag{52}$$

Thus there are five equations, equations (43) through (45) and equations (22) and (33), and five dependent variables f, ρ, T, C, and H. We normally need seven boundary conditions for the present equations (43) through (45). There are, however, eight boundary conditions in the present analysis. The extra boundary condition is needed because the quantity η_s is an addition unknown. Now we see that the equations (43) through (52) and the equations (22) and (33) together constitute a consistent system for a boundary value problem. The solution of the transformed equations will be obtained numerically with the use of a digital computer.

As was mentioned in the Introduction, the numerical integration of the equations requires considerable care because of the split boundary conditions and, most of all, the nonequilibrium chemical effect. In order not to complicate further the numerical work, here it is assumed that

$$\frac{\rho\mu}{\rho_s\mu_s}=1 \tag{53}$$

for the entire stagnation-point shock layer. Assumption (53) should not introduce any undue error into the heat-transfer results since it is the value of $\rho\mu$ in the order of that near the shock which controls the heat transfer (see ref. 15). The degree of approximation involved in the present analysis due to assumption (53) will probably be of the same order as that involved in the hypersonic boundary-layer work of reference 21 with the similar assumption. The analysis of reference 21 has been shown to be satisfactory for engineering purposes in comparison with the exact boundary-layer solution of reference 7.

The properties of free-stream air used in the numerical analysis are obtained from reference 22. The Prandtl number is assumed to be 0.72 in the present solution.

The heat transfer is obtained from the solution of the equations as

$$q_{SL}=2^{1/4}\frac{1}{Pr}\sqrt{\rho_s\mu_s}\sqrt{\frac{u_\infty}{L}}h_{t,\infty}H_w' \tag{54}$$

RESULTS AND DISCUSSION

Figures 2, 3, and 4 show three of the typical solutions of the conservation equations. All the figures are for a flight speed of 26,000 ft/sec, a nose radius of 1 foot, and a noncatalytic wall temperature of 1500 K.

As was shown in reference 3, the vorticity interaction which accompanies the thickening of the boundary layer begins to have a first-order effect on the skin friction and heat transfer at the Knudsen number range corresponding to the present flight at 250,000 feet altitude. The velocity and the enthalpy profiles given in figure 3 show the thickened boundary layer. Figure 4 shows that the entire shock layer becomes quite viscous at a flight altitude of 280,000 feet. The enthalpy profile shows that the effect of the cooled wall is felt by most of the shock layer at this flight condition.

The chemical state of the shock layer can be seen from the temperature and the atom mass-fraction profiles of figures 2, 3, and 4. In the conventional boundary-layer analysis, it has been assumed that the air is dissociated to its adiabatic equilibrium state at the edge of the boundary layer. The broken lines in figures 2, 3, and 4 show the temperatures and the atom mass fractions which would be attained if the air were to reach equilibrium before the cooling effect of the wall is felt. A study of the temperature and the atom mass fraction profiles in the light of the adiabatic equilibrium values of temperature and mass fraction shows that the entire shock layer is considerably out of equilibrium already at an altitude of 230,000 feet. As will be seen later in figure 5, the nonequilibrium chemical reaction in the shock layer at an altitude of about 230,000 feet causes a first-order deviation in the heat transfer from that calculated with the conventional assumption

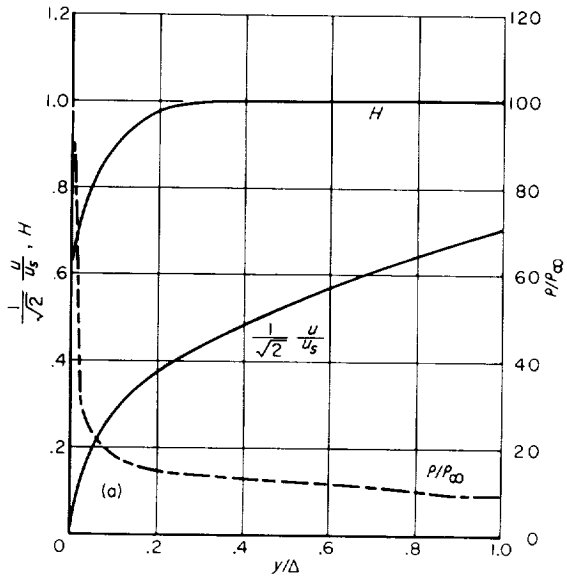

(a) Velocity, enthalpy, and density profiles.

FIGURE 2.—Typical solutions of conservation equations for u_∞=26,000 feet per second, L=1 foot; T_w=1,500° K, and altitude=230,000 feet, Re=16,680.

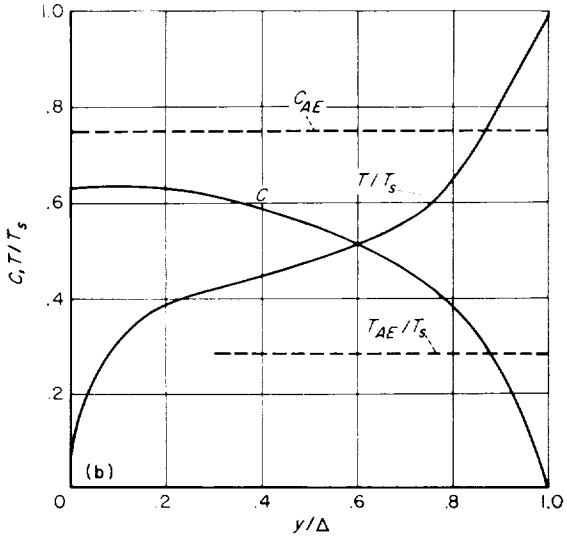

(b) Temperature and atom mass-fraction profiles.

FIGURE 2.—Concluded.

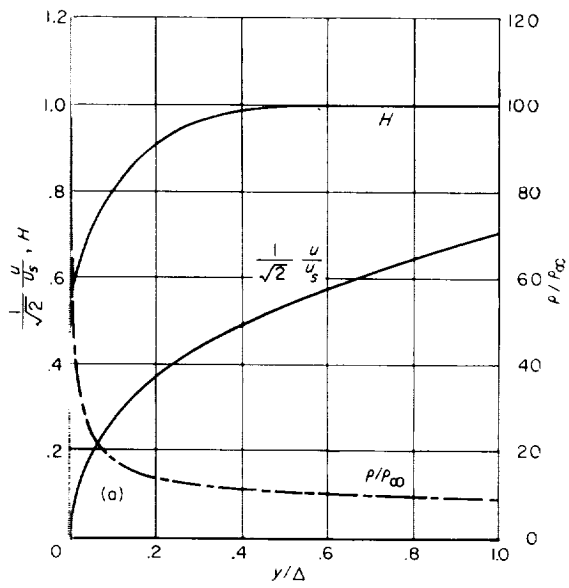

(a) Velocity, enthalpy, and density profiles.

FIGURE 3.—Typical solutions of conservation equations for u_∞=26,000 feet per second, L=1 foot, T_w=1,500° K, and altitude=250,000 feet, Re=7,590.

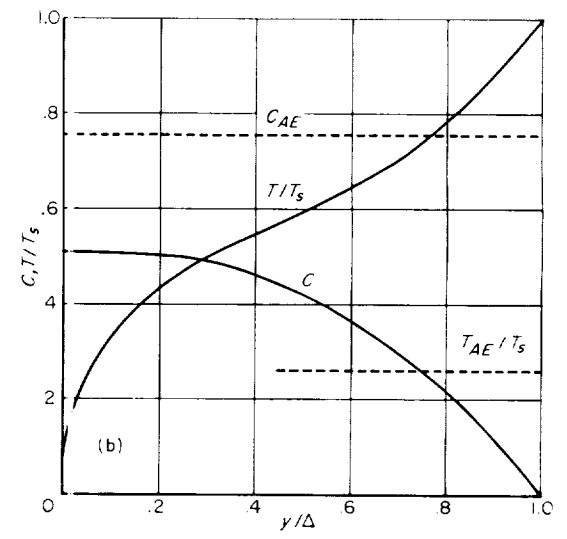

(b) Temperature and atom mass-fraction profiles.

FIGURE 3.—Concluded.

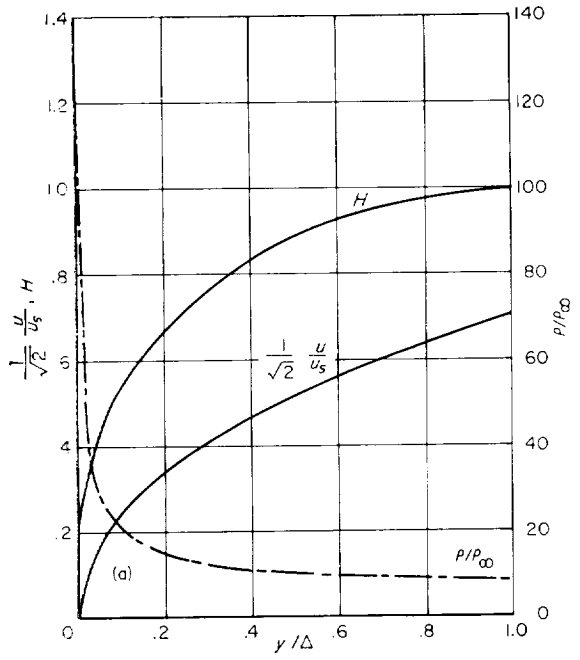

(a) Velocity, enthalpy, and density profiles.

FIGURE 4.—Typical solutions of conservation equations for $u_\infty = 26{,}000$ feet per second, $L = 1$ foot, $T_w = 1{,}500°$ K, and altitude = 280,000 feet, $Re = 1{,}615$.

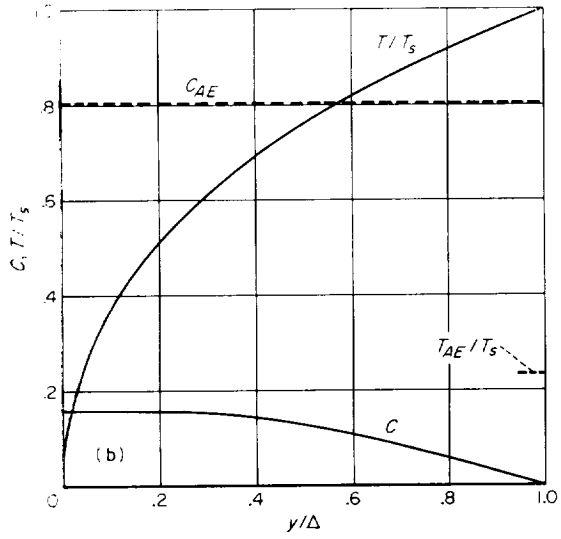

(b) Temperature and atom mass-fraction profiles.

FIGURE 4.—Concluded.

of equilibrium boundary-layer-edge conditions. It should be remembered that the vorticity interaction also begins to have a first-order effect on heat transfer at the similar flight condition (about 250,000 ft). At the altitude of 280,000 feet (fig. 4), it is seen that most of the shock layer is nearly frozen.

Figure 5 shows the effect of the chemical reaction on stagnation point heat transfer as a function of the flight altitude. The ordinate $(q/q_E)_{BL}$ is obtained, in the present analysis, by the approximate relationship,

$$\left(\frac{q}{q_E}\right)_{SL} = \frac{h_s - h_w}{h_s - h_{w,E}} \tag{55}$$

The use of the above equation is justified here by the following argument. Our experience with the chemically reacting boundary layers and the comparison of the analyses of incompressible and compressible viscous shock layers found in references 1 and 3, respectively, show that the heat-transfer results are not greatly affected by the detailed variation of the fluid properties through the flow field. The main effect, therefore, of the chemical reaction on heat transfer to a noncatalytic wall appears through the driving potential $(h_s - h_w)$.

Figure 5 contains results for $u_\infty = 26{,}000$ ft/sec and a result for $u_\infty = 30{,}000$ ft/sec. Let us first consider the results for $u_\infty = 26{,}000$ ft/sec. The solid line shows the heat-transfer ratio $(q/q_E)_{SL}$ for

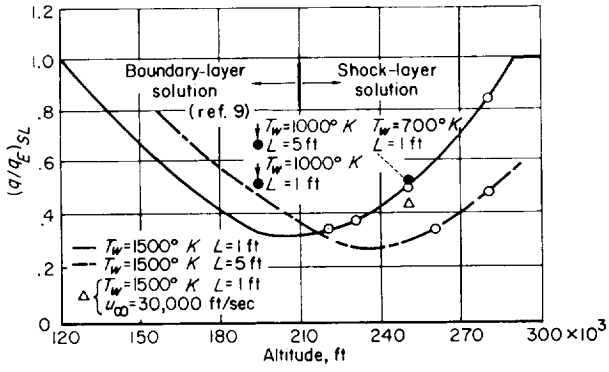

FIGURE 5.—Effect of chemical reaction on heat transfer to noncatalytic wall; $u_\infty = 26{,}000$ ft/sec unless otherwise specified.

the nose radius of 1 foot and the wall temperature of 1500° K. It is first seen from the solid line that the shock-layer dissociative chemical reaction reduces the heat transfer by the maximum relative amount when the flight altitude is about 210,000 feet. At this altitude, the air dissociates essentially to its equilibrium state at the edge of the boundary layer. The boundary-layer reaction, which is a recombination process, on the other hand, is almost completely frozen at this flight condition as was seen in reference 9. The shock layer dissociative relaxation and the near frozen boundary-layer recombination process together reduce the heat transfer by the maximum relative amount at the altitude of 210,000 feet. The heat-transfer ratio increases as the altitude deviates in either direction from the optimum height of 210,000 feet. The heat-transfer ratio increases at the lower altitudes as the recombination process increases in the boundary layer. At the higher altitudes, on the other hand, the heat-transfer ratio $(q/q_E)_{SL}$ is increased as a smaller portion of the total energy becomes associated with the chemical energy of dissociation. This is because the degree of dissociation in the shock layer becomes smaller as the dissociative relaxation time increases with altitude. The relaxation time increases as the pressure is decreased and also as the cooling effect of the wall is felt by a greater portion of the shock layer at the increased Knudsen number (see fig. 4). It can be said from the preceding discussion that the dissociative relaxation in the shock layer is the controlling chemical reaction for heat transfer at the altitudes above about 210,000 feet, whereas it is the boundary-layer recombination which controls the heat transfer at the lower altitudes. The broken line in figure 5 is for the same conditions as the solid line except that the body nose radius is 5 feet. It is seen that the increased nose radius displaces the $(q/q_E)_{SL}$ curve to a higher altitude. The displacement is greater in the dissociation-controlled region than in the recombination-controlled region of lower altitudes. This means that the variation of the nose radius influences the shock-layer reaction more than it does the boundary-layer reaction. The main reason for this lies in the fact that the shock-layer thickness is approximately proportional to the nose radius, whereas the boundary-layer thickness is proportional to the square root of the radius. It is seen that the air practically dissociates to the equilibrium state at the edge of the boundary layer at the approximate altitude of 240,000 feet when the nose radius is 5 feet.

The effects of the wall temperature on the heat-transfer ratio $(q/q_E)_{SL}$ are shown in figure 5 by the filled symbols. At the altitude of 250,000 feet and for the nose radius of 1 foot, it is seen that the wall temperature has little effect on the dissociative process in the shock layer. It is because the domain of influence of the wall temperature is still rather confined to the regions near the wall as seen by the enthalpy profile of figure 3. As the altitude and therefore the Knudsen number is increased, however, it is expected that the effect of the wall temperature will be felt by a greater portion of the shock layer (fig. 4) and, therefore, the effect of the wall temperature on the chemical reaction will become greater. The wall temperature is seen to have a considerable effect on the heat transfer through its effect on the boundary-layer recombination process at the lower altitudes. The boundary-layer reaction is influenced by the wall temperature substantially and this point was brought out in reference 9.

A shock-layer solution for $u_\infty = 30{,}000$ ft/sec is shown in figure 5 for a nose radius of 1 foot, wall temperature of 1500° K, and altitude of 250,000 feet. It is seen that the relative effect of the chemical reaction on heat transfer is not too sensitive to the speed in the present flight regime.

Before leaving figure 5, it may be important to note that the chemical reaction of dissociation and recombination in the stagnation-point shock layer ceases to be a problem above altitudes of about 300,000 feet.

We have, so far, mainly discussed the effect of the chemical reaction on heat transfer. We have seen that the thickening of the boundary layer which accompanies the rarefaction of air has a large effect on the shock-layer chemical reaction. Besides its effect on the chemical reaction, the thickening of the boundary layer increases the heat transfer directly. In figure 6, we shall see the simultaneous effect of the chemical reaction and the air rarefaction on the heat transfer. The curve of $(q/q_E)_{SL}$ versus altitude showing the chemical reaction effects alone is transferred from figure 5 as the dashed line curve on figure 6. This

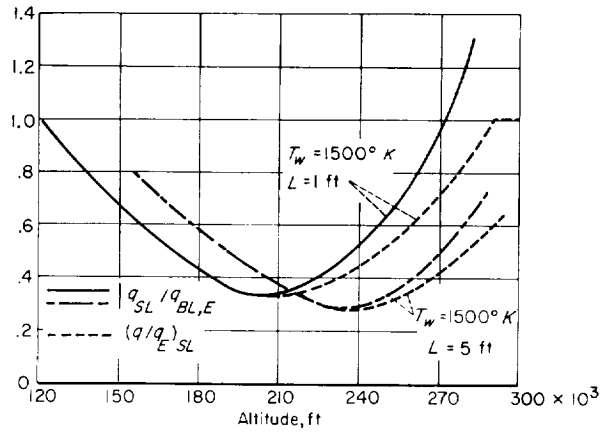

FIGURE 6.—Simultaneous effect of chemical reaction and air rarefaction on heat transfer to noncatalytic wall; $u_\infty = 26{,}000$ ft/sec.

ratio $(q/q_E)_{SL}$ shows only the chemical reaction effects because rarefaction effects occur in both the numerator and denominator. When the heating rate q_{SL} is normalized by the heating rate, $q_{BL,E}$, obtained from conventional equilibrium boundary-layer theory, the ratio $q_{SL}/q_{BL,E}$ will show the combined nonequilibrium chemical and rarefaction effects since conventional equilibrium bounday-layer theory considers neither phenomenon. This ratio is shown in figure 6 for two nose radii. The abscissa is again the flight altitude. From the present heat-transfer relationship (eq. (54)), and that given in reference 7, it is obtained that

$$\frac{q_{SL}}{q_{BL,E}} = \frac{1.756}{\sqrt{\beta_0}} \frac{H_w'}{1-H_{w,E}} \tag{56}$$

The streamwise velocity gradient at the edge of the boundary layer, β_0, is obtained from the equation given by reference 23, as

$$\beta_0 = \sqrt{\epsilon(2-\epsilon)}$$

where the density ratio ϵ is here calculated by assuming that the air is in equilibrium immediately behind the shock.

At the lower altitudes, the classical boundary-layer theory is essentially valid and, therefore, the heat-transfer ratio $q_{SL}/q_{BL,E}$ is the same as the ratio $(q/q_E)_{SL}$. At the higher altitudes, figure 6 shows that the heat-transfer ratio $q_{SL}/q_{BL,E}$ becomes higher than the ratio $(q/q_E)_{SL}$ as the result of the direct effect of the air rarefaction (vorticity interaction) on heat transfer. On the solid curve corresponding to the 1-foot nose radius we note that at about 270,000 feet, the heat transfer is the same as that which would be calculated from conventional equilibrium boundary-layer theory. The reason is that the non-equilibrium chemical and air rarefaction effects which cause the heat transfer to deviate (in opposite directions) from the equilibrium boundary-layer value are just in balance and counteract one another at that point. At the altitudes below 270,000 feet, it is seen that the effect of the chemical reaction dominates over the direct effect of the air rarefaction, whereas the reverse is true at the higher altitudes. A similar trend occurs when the nose radius is 5 feet but at higher altitudes as shown in the figure.

Finally, let us consider the simultaneous effect of the chemical reaction and the air rarefaction on the shock-layer thickness. The solid line and the filled points in figure 7 show the results of the present analysis. Figure 7 also contains the shock-layer thicknesses calculated by other investigators for different conditions, which are shown here for the purpose of comparison. The shock-layer thicknesses based on the conventional inviscid flow theory are shown for $\epsilon = 0.11$ and for ϵ based on the assumption of an equilibrium gas behind the shock. These values are obtained from reference 23. The shock-layer thickness calculated in reference 3 for the viscous compressible but chemically inert gas is also shown in the figure. It is seen from the results of reference 3 that the shock layer becomes thinner as the air becomes rarefied and the effect of the cooled wall is felt by the greater portion of the shock layer. The result

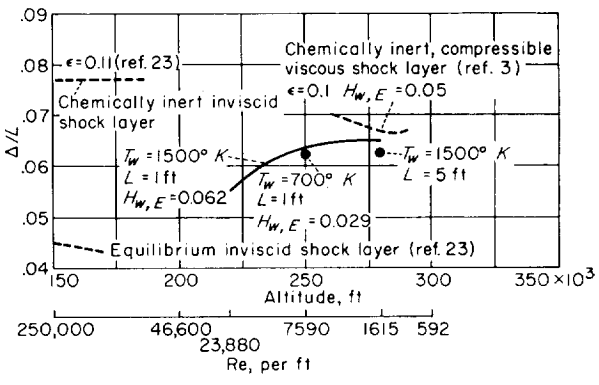

FIGURE 7.—Thickness of viscous nonequilibrium shock layer; $u_\infty = 26{,}000$ ft/sec.

of the present analysis, on the other hand, shows that the shock-layer thickness increases as the air becomes rarefied. The explanation of this phenomenon is as follows. As the air is being rarefied, the shock-layer thickness is affected in two opposite ways. First, the cooling effect of the wall is felt by the greater portion of the shock layer and the shock layer tends to become thinner. With the rarefaction, however, the dissociative chemical reaction rate becomes slower and the degree of dissociation becomes smaller. The shock-layer thickness therefore tends to increase with the rarefaction of air. The over-all effect of the air rarefaction is that the chemical effect dominates over the cooled wall effect and the shock layer becomes thicker as the Reynolds number is decreased in the present flight regime.

CONCLUDING REMARKS

The nonequilibrium chemical reaction of dissociation and recombination is studied theoretically for air in the viscous shock layer at the stagnation region of axisymmetric bodies. The flight regime considered is for speeds near satellite speed and for altitudes between 200,000 and 300,000 feet.

As altitude is increased from 200,000 to 300,000 feet, the flow in the shock layer varies from one which supports a well-defined boundary layer to one characterized by a thick viscous layer. The chemical reaction rate, at the same time, varies from near equilibrium to completely frozen.

The nonequilibrium chemical reaction is found to produce a significant reduction in the heat transfer to noncatalytic walls at certain altitudes. For a wall temperature of 1500° K and nose radius of 1 foot the significant altitude lies between about 150,000 and 270,000 feet. The maximum reduction in heat transfer occurs at about 210,000 feet altitude and the heat transfer is then about one-third of the equilibrium value.

It is shown that the controlling chemical reaction for heat transfer at higher altitudes is the dissociative shock-layer reaction, whereas at lower altitudes it is the boundary-layer recombination process.

The air at the boundary-layer edge is found to be in a state of chemical equilibrium below altitudes between 210,000 and 240,000 feet for nose radii from 1 to 5 feet. Most of the shock layer, however, is found to be substantially out of equilibrium throughout the flight regime considered. It can be said from this that the radiation characteristics from the shock layer may be considerably different from that calculated with the assumption of an equilibrium shock layer. Also, the gas which surrounds a vehicle and the gas at the wake and trail of the vehicle probably contain substantially less amounts of dissociated radicals than they would if the stagnation shock layer were in equilibrium.

The relative effect of chemical reaction on heat transfer is found to be rather insensitive to flight speed.

Nose radius is seen to affect the dissociative chemical reaction in the shock layer more than it does the recombination process in the boundary layer. The wall temperature, on the other hand, influences the boundary-layer reaction at lower altitudes most significantly, and the shock-layer dissociative reaction at extremely high altitudes moderately. At intermediate altitudes, however, the effect of wall temperature on chemical raction is negligible.

As the altitude is increased, rarefaction of the air is found to produce two opposite effects on the shock-layer thickness. First, the effect of the cooled wall is felt by a greater portion of the shock layer and the shock layer tends to become thinner. The rarefaction, at the same time, freezes the dissociative chemical reaction which tends to increase the thickness. The overall effect of the air rarefaction on the shock-layer thickness is that the chemical effect dominates over the cooled wall effect and the shock layer becomes thicker as the air is rarefied. Finally, the chemical reaction kinetics at the temperatures above about 7000° K are not well known at the present time. The present results, therefore, should be considered with this fact in mind.

AMES RESEARCH CENTER
NATIONAL AERONAUTICS AND SPACE ADMINISTRATION
MOFFETT FIELD, CALIF., *May 8, 1961*

APPENDIX A

ITERATION PROCEDURE AND NUMERICAL SOLUTION OF CONSERVATION EQUATIONS

Some of the basic principles programmed into the digital computer to solve equations (43), (44), and (45) are discussed in this appendix.

A conventional, straightforward iteration technique is used to integrate the momentum and the energy equations. The solution of the momentum equation begins with the guessing of a function $\rho(\eta)$. The two known boundary conditions (eq. (46)) are then applied, and a third boundary condition $f''(0)$ is guessed at the wall. The forward integration then begins and continues until one of the two boundary conditions, say equation (49), is satisfied. At this point, the other boundary condition (50) is checked to see if it is also satisfied. If the boundary condition (50) is not satisfied, then another value of $f''(0)$ is guessed and the equation is again integrated. The iteration thus continues on the boundary condition (50), with the aid of $f''(0)$, until all the boundary conditions are satisfied. The solution of the momentum equation gives η_s as well as $f(\eta)$ and its derivatives. The method of solution of the energy equation is quite similar. For a given wall temperature, C_w is guessed and this yields the boundary condition H_w with the aid of equation (47). Another boundary condition $H'(0)$ is guessed at the wall and the forward integration begins. The integration continues to η_s at which point a check is made to see if the boundary condition (51) is satisfied. If not, a new guess is made on $H'(0)$ and the integration is repeated. The iteration is continued until all the boundary conditions are satisfied.

The diffusion equation (45) is not amenable to such straightforward iteration procedure. There are essentially two categories of difficulties one must face in order to solve the equation successfully.

The first category of difficulty arises with the increasing magnitude of the reaction rate term $(L/u_\infty)(W/\rho)$. As the magnitude of the chemical reaction term $(L/u_\infty)(W/\rho)$ is increased, the equation fails to converge unless almost exactly the correct value of C_w has been guessed and $H(\eta)$ has been obtained. For most of the reasonable values guessed, not only does the equation fail to converge but it diverges even before the integration can reach η_s. To circumvent this difficulty, the following procedure was used in the present analysis. The equation to be solved is

$$\frac{1}{Pr}C''+2fC'=-\frac{1}{\sqrt{2}}\left(\frac{L}{u_\infty}\right)\left(\frac{W}{\rho}\right) \tag{45}$$

with the boundary conditions

$$C'(0)=0 \tag{48}$$

$$C(\eta_s)=0 \tag{52}$$

The main trouble here is caused by the nonlinear effect of the term $(L/u_\infty)(W/\rho)$. The energy and the diffusion equations are iterated together in the present endeavor. With $f(\eta)$ known from the solution of equation (43), diffusion equation (45) is linear for each iterative step if (W/ρ) is calculated from the values of T and C obtained from the preceding iteration of the energy and diffusion equations. Therefore, for the nth iteration step and for a given $f(\eta)$ we shall linearize the diffusion equation as

$$\frac{1}{Pr}C_n''+2fC_n'=-\frac{1}{\sqrt{2}}\frac{L}{u_\infty}\left(\frac{W}{\rho}\right)_{n-1}\Gamma \tag{A1}$$

with the boundary conditions

$$C_n'(0)=0 \qquad C_n(\eta_s)=0 \tag{A2}$$

The symbol Γ represents a positive number between 0 and 1, and is put in here to further insure the convergence. During the iteration for a particular n, if the diffusion equation diverges before η reaches η_s, the computer is programmed to reduce the effect of W/ρ by reducing Γ until the integration can be accomplished satisfactorily. The results for the reduced Γ are then used to calculate a new W/ρ, and the diffusion equation is rein-

tegrated for a new Γ which is greater than the preceding one by a certain suitable amount. The solution of equation (A1) for the particular n is built up, in this manner, until Γ becomes unity. When Γ becomes unity, the simultaneous iteration of the energy and the diffusion equations resumes. The iteration of the two equations continues until they converge. The function $\rho(\eta)$ is then recalculated and the momentum equation is solved with the new $\rho(\eta)$. The final solution of the problem is obtained when all three equations converge simultaneously.

The second category of difficulty arises during the course of the iterations explained above. The difficulty is associated with the additional iteration required to satisfy the split boundary conditions (A2) of the diffusion equation. To circumvent this difficulty, we express the solution of equation (A1) by

$$C_n(\eta)=B_nC_{c,n}(\eta)+C_{p,n}(\eta) \tag{A3}$$

The above expression is permissible because equation (A1) is linear. The symbol $C_{c,n}(\eta)$ represents the complementary function, whereas $C_{p,n}(\eta)$ represents the particular solution. The function $C_{c,n}$, therefore, is a solution of the homogeneous equation

$$\frac{1}{Pr}C_{c,n}''+2fC_{c,n}'=0 \tag{A4}$$

whereas $C_{p,n}$ is a solution of the nonhomogeneous equation

$$\frac{1}{Pr}C_{p,n}''+2fC_{p,n}'=-\frac{1}{\sqrt{2}}\frac{L}{u_\infty}\left(\frac{W}{\rho}\right)_{n-1}\Gamma \tag{A5}$$

We obtain solutions $C_{c,n}$ and $C_{p,n}$ to satisfy the following boundary conditions, respectively, all at $\eta=0$,

$$\left.\begin{aligned}C_{c,n}(0)&=1\\C_{c,n}'(0)&=0\end{aligned}\right\} \tag{A6}$$

$$\left.\begin{aligned}C_{p,n}(0)&=0\\C_{p,n}'(0)&=0\end{aligned}\right\} \tag{A7}$$

We also let

$$B_n=-\frac{C_{p,n}(\eta_s)}{C_{c,n}(\eta_s)} \tag{A8}$$

Now it is seen that (A3) is the complete solution of equation (A1) which satisfies the boundary conditions (A2). Let us now examine equations (A4) and (A5). An examination of equation (A4) in the light of the boundary conditions (A6) shows that the unique solution of the homogeneous equation is $C_{c,n}(\eta)=1$. The complete solution for the nth iterated equation (A1) can therefore be written as

$$C_n(\eta)=-C_{p,n}(\eta_s)+C_{p,n}(\eta) \tag{A9}$$

The integration which must be performed for the diffusion equation with a digital computer is now reduced to the integration of equation (A5) with the boundary conditions (A7). The boundary conditions (A7) are both given at $\eta=0$ and, therefore, no iteration is involved in the solution of equation (A5).

REFERENCES

1. Probstein, R. F., and Kemp, N. H.: Viscous Aerodynamic Characteristics in Hypersonic Rarefied Gas Flow. Jour. Aero/Space Sci., vol. 27, no. 3, March 1960, pp. 174–192.
2. Hoshizaki, H., Neice, S., and Chan, K. K.: Stagnation Point Heat Transfer Rates at Low Reynolds Numbers. IAS Paper No. 60-68, 1960.
3. Ho, Hung-Ta, and Probstein, Ronald F.: The Compressible Viscous Layer in Rarefied Hypersonic Flow. Brown Univ., Div. of Engineering, ARL TN 60-132, Aug. 1960.
4. Li, T. Y.: Nonequilibrium Flow in Gas Dynamics. Rensselaer Polytechnic Inst., TR AE 5901, May 1959. Also, ARS Preprint 852-59, June 1959.
5. Freeman, N. C.: Non-Equilibrium Flow of an Ideal Dissociating Gas. Jour. Fluid Mech., vol. 4, pt. 4, Aug. 1958, pp. 407–425.
6. Lick, W.: Inviscid Flow Around a Blunt Body of a Reacting Mixture of Gases. Part A—General Analysis. Rensselaer Polytechnic Inst., TR AE 5810, May 1958. Part B—Numerical Solutions. Rensselaer Polytechnic Inst., TR AE 5814, Dec. 1958.
7. Fay, J. A., and Riddell, F. R.: Theory of Stagnation Point Heat Transfer in Dissociated Air. Jour. Aero/Space Sci., vol. 25, no. 2, Feb. 1958, pp. 73–85, 121.
8. Kemp, Nelson H., Rose, Peter H., and Detra, Ralph W.: Laminar Heat Transfer Around Blunt Bodies in Dissociated Air. Jour. Aero/Space Sci., vol. 26, no. 7, July 1959, pp. 421–430.
9. Chung, Paul M, and Anderson, Aemer D.: Heat Transfer Around Blunt Bodies With Nonequilibrium Boundary Layers. Proc. 1960 Heat Transfer and Fluid Mechanics Institute, pp. 150–163.

10. Goodwin, Glen, and Chung, Paul M.: Effects of Nonequilibrium Flows on Aerodynamic Heating During Entry Into the Earth's Atmosphere From Parabolic Orbits. Preprint. Second International Congress for Aeronautical Sciences held at Zurich, Switzerland, Sept. 1960.
11. Camm, J. C., Kivel, B., Taylor, R. L., and Teare, J. D.: Absolute Intensity of Non-Equilibrium Radiation in Air and Stagnation Heating at High Altitudes Rep. 93, AVCO Res. Lab., Everett, Dec. 1959.
12. Goulard, Madeleine, and Goulard, Robert: The Aerothermodynamics of Reentry Trials. ARS Preprint 1145–60, May 1960.
13. Tsien, H. S.: Superaerodynamics, Mechanics of Rarefied Gases. Jour. Aero. Sci., vol. 13, no. 12, Dec. 1946, pp. 653–664.
14. Stalder, Jackson R., Goodwin, Glen, and Creager, Marcus O.: A Comparison of Theory and Experiment for High-Speed Free Molecule Flow. NACA Rep. 1032, 1951.
15. Hayes, Wallace D., and Probstein, Ronald F.: Hypersonic Flow Theory, Academic Press, New York, 1959.
16. Hansen, C. Frederick: Approximations for the Thermodynamic and Transport Properties of High-Temperature Air. NASA TR R–50, 1959.
17. Guggenheim, E. A.: Boltzmann's Distribution Law. Interscience Publishers, Inc., N.Y., 1955.
18. Lighthill, M. J.: Dynamics of a Dissociating Gas. Part 1. Equilibrium Flow. Jour. Fluid Mech., vol. 2, 1957, pp. 1–32.
19. Wray, K., Teare, J. D., Kivel, B., and Hammerling, P.: Relaxation Processes and Reaction Rates Behind Shock Fronts in Air and Component Gases. AVCO Res. Rep. 83, Dec. 1959.
20. Camac, M., and Vaughan, A.: Oxygen Vibration and Dissociation Rates in Oxygen-Argon Mixtures. AVCO Res. Rep. 84, Dec. 1959.
21. Lees, Lester: Laminar Heat Transfer Over Blunt-Nosed Bodies at Hypersonic Flight Speeds. Jet Propulsion, vol. 26, no. 4, Apr. 1956, pp. 259–269.
22. Minzner, R. A., and Ripley, W. S.: The ARDC Model Atmosphere, 1956. AF CRC TN 56–204, Dec. 1956.
23. Li, T. Y., and Geiger, R. E.: Stagnation Point of a Blunt Body in Hypersonic Flow. Jour. Aero. Sci., vol. 24, Jan. 1957, pp. 25–32.

U.S. GOVERNMENT PRINTING OFFICE: 1961